Reduction of Electron Beam Induced Radiation Damage of Organic Material by Cooling to 4 K (Cryo Electron Microscopy)

I. Dietrich
Forschungslaboratorien der Siemens AG

E. Knapek
Forschungslaboratorien der Siemens AG

G. Lefranc
Forschungslaboratorien der Siemens AG

Utah State University
MERRILL-CAZIER LIBRARY

REDUCTION OF ELECTRON BEAM INDUCED RADIATION DAMAGE OF ORGANIC MATERIAL BY COOLING TO 4 K (CRYO ELECTRON MICROSCOPY)

I. Dietrich, E. Knapek, G. Lefranc

Forschungslaboratorien der Siemens AG, Postfach 83 09 52,
D-8000 München 83, West Germany
Phone No. 089 636 45160

Abstract

Structure investigations of organic, in particular biological, material are frequently performed with a strong electron beam. If the dose is higher than $1e/\text{Å}^2$, as required e.g. for high resolution electron microscopy, the results are strongly influenced by radiation damage. There are no means for preventing breaking of chemical bonds and ionizing of atoms and fractures of molecules due to the electron impact. The secondary processes, however, such as diffusion or evaporation of the fragments, can be strongly reduced by cooling the specimen to 4 K (cryoprotection). A suitable instrument for experimenting with cryoprotection is a microscope equipped with a superconducting lens system.

Topics relevant for cryomicroscopy are: instrumentation; determination of cryoprotection factors of various materials by electron diffraction; direct imaging in particular for information on the steric structure of the material; preparation conditions for an effective cryoprotection.

Though the knowledge of the physics and chemistry causing radiation damage at 4 K is still limited, a useful application of cryoprotection is already possible.

Introduction

The interaction of the electron beam with organic material consists of a transfer of energy of ~ 100 eV per electron and impact, which causes excited states in the molecules, ionization and breaking of chemical bonds (energy 10 eV). As a consequence free radicals are present which may undergo chemical processes. They may also migrate to sinks. Especially ionized hydrogen, whose mobility is extremely high, will diffuse to other molecules and in general oxidation (removal of an electron) and reduction (addition of an electron) may occur. Secondary electrons escape from the specimen. Macroscopically we observe charging. With increasing dose, depending on the physical properties of the specimen, heating and mass loss may occur, since elements such as hydrogen, oxygen and nitrogen and to a lesser extent carbon are evaporated. As a consequence of the rearranging of atoms, the crystallinity--more generally the order on the atomic level of the material--is increasingly destroyed.

The effect is somewhat different on aliphatic and on aromatic compounds. Aliphatic compounds are either broken into smaller parts or polymerized if C-H bonds are still available. Aromatic compounds just lose substituents on the aromatic ring in the beginning and therefore are more radiation resistant.

The interaction of the electrons with thin films (~ 10 nm thick) of organic material is the weaker the higher the energy of the incident electrons chosen, and in order to relate all investigation to the same electron beam voltage V we assume for a first approximation that the interaction is proportional to $V^{-1/2}$.

The change in structure due to electron impact may be desired. Some polymerization processes of hydrocarbons, e.g. take place as a consequence of irradiation. In electron microscopy, however, this change is called radiation damage and it is the most serious handicap for the determination of the morphology of organic specimens if a resolution on the order of a few Ångstroms is required.

Electron Beam Induced Damage in Electron Microscopy

Experimental Results
Fig. 1 gives an example of the change in a

high resolution image due to radiation damage (Murata 1978). The specimen consists of chlorinated Cu-phthalocyanine, one of the most radiation insensitive organic materials, which has been investigated in many laboratories, particularly in Japan. The pattern on the micrograph can be coordinated to the crystal structure of the specimen on the atomic level. The first micrograph of the series taken with a relatively low dose shows several spots in different stages of damage. With increasing dose the damaged regions extend, and major disarrangement of the molecules starts, where there are lattice defects (in the environment of A and B). The light optical diffractograms of different regions in the micrograph permit a half quantitative estimation of the degree of disorder in the different regions. In this way we can study the damage in detail and speculate about the chemical and physical processes responsible.

Unfortunately the materials we normally deal with are at least two orders more radiation sensitive, and the dose we need for a high resolution image with sufficient contrast ($\sim 10^4$ e/nm^2 for 0.3 nm resolution by application of the most sensitive photographic emulsion) is so high that, apart from carbonized residuals, nothing is left of the original structure.

There are several possibilities in order to measure the radiation sensitivity of the normal organic material, where we obtain the average value over a larger region as described e.g. by Isaacson (1977). The most popular method, if the material crystalizes, is electron diffraction. The fading of the reflections with increasing dose proves the start of the disarrangement of the atoms. If we draw conclusions in analogy to the results in Fig. 1 we have e.g. to assume that the disappearance of the higher-order reflections means a limitation of the resolution. But there might still be small regions where the structure is intact. On the other hand, if just the first-order reflections remain and all the other reflections have faded the degree of disorder is probably so high that even with the help of image reconstruction the original structure cannot be extracted from the image.

For controlling the vanishing of the crystallinity one can also observe the disappearance of the extinction lines in bright field and dark field images. There are, however, many possibilities for errors in this method. A further method for measuring the changes due to electron impact is electron energy loss spectroscopy. In this case the destruction of certain molecular bonds can be judged by the flattening of the coordinated peaks. An indication for the radiation damage also gives the mass loss which can be detected by a change in transparency of the object or with a radioactive tracer method. The results do not tell us anything about the kind of structure deterioration. The morphology, of course, must have changed.

In order to illustrate the order of magnitude of the radiation damage a few examples of vanishing dose values D_v, i.e. the dose which causes a complete destruction of the reflections, are listed in Table 1. The dose response strongly depends on the measuring method as is demonstrated in Fig.2.

Efforts in Order to Avoid the Damage

In order to reduce the radiation damage elaborate preparation techniques were developed. Staining is often used. In the case of negative staining, compounds with high atomic weight e.g. uranylacetate solved in water are brought in contact with the specimen. The solution penetrates into the holes of the organic material and provides contrasts of the substructure. The staining means also a fixation of the specimen. Even if the organic material is destroyed by the electron beam, the heavy metal atoms remain in their original position. If positive staining is applied the heavy metal atoms are bound to the organic object. In any case the metal compounds form clusters which often grow due to the electron impact and the resolution is limited by their diameter, which is 1 to 2 nm. These resolution limitations are also valid in every case where the contrast is enhanced by shadowing the object or its replica with heavy metals after a certain treatment. These decoration methods were much improved but at higher resolution the metal clusters are artefacts which make it difficult to recognize the morphology. The same is true if one works with techniques in which the treatment of the specimen is connected with cooling such as freeze drying, freeze etching and freeze fracture, since afterwards the object is decorated with heavy atoms.

In the last few years a real improvement has been gained by embedding biological material in glucose or similar matrices. For high resolution a minimum dose technique is required where the object is exposed to $\simeq 100$ e/nm^2 so that almost no contrast is produced on the photographic film (Unwin and Henderson 1975). The pattern can only be obtained with the help of image reconstruction. It requires much effort to perform this technique but worthwhile results were obtained. After nearly ten years of research in laboratories all over the world a resolution of $\simeq 0.3$ nm was achieved on purple membrane (Haywardt and Stroud 1981). When the reduction of the radiation damage with decreasing temperatures was discovered by radiochemical investigations in the late sixties (Box 1975), one wanted to take advantage of this effect in electron microscopy. In the following chapters we report on the instrument used for this purpose and on the results obtained with electron microscopy on cold specimens.

Instruments for Investigation of Beam Damage at Low Temperatures

Cold Stages

Cooling of the specimen down to liquid helium was attempted with the help of cold stages. A real chance to obtain $\simeq 4$ K (4.2 K = boiling point of liquid helium at atmospheric pressure) is only given if elaborate devices consisting of a bath cryostat, where the specimen is surrounded by "4 K walls," are available. A cold stage of this type designed by the Boersch group in Berlin is demonstrated in Fig. 3. In most cases specimen holders cooled with evaporating liquid helium were applied (e.g. as in Fig. 4). In this case the mechanical stability was in general moderate, and for this reason high resolution images could not
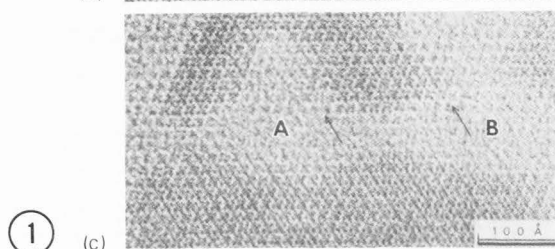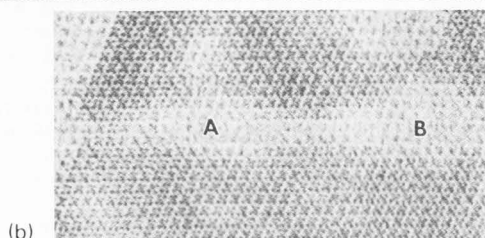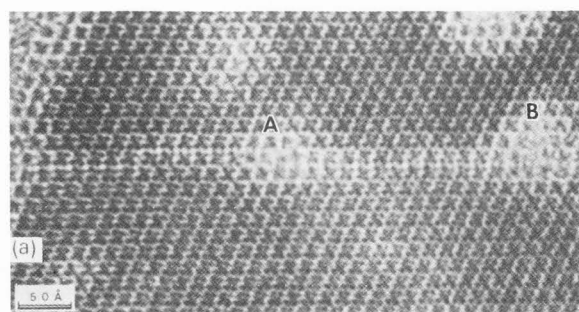
Fig. 1. Damage series of chlorinated Cu phtalocyanine (Murata 1978). Beam voltage 100 kV, electron optical magnification 150,000, overfocus 60 nm (reversed contrast).

The damage starts near the crystal defect, a slip along [110]. The initial damage sites are marked with A and B (Fig. 1a). With increasing electron dose the damaged area first propagates along the defect, then extends to both sides (Fig. 1b and c).

Fig. 2. Dose response of a thin L-histidine film (Isaacson 1977). 1. Loss of crystallinity (electron diffraction technique, lower scale on abscissa). 2. Loss of mass (change in image intensity, upper scale). 3. Damage of the aromatic ring (electron energy loss spectroscopy, change in 0-10 eV structure, upper scale).

Fig. 3. He cryostat for specimen cooling (Siegel 1972).

Fig. 4. Specimen holder cooled with liquid helium for high voltage microscopes with side-entry specimen stage (Thomas et al. 1974). Although this holder was constructed for tension experiments, it gives an impression of the principle of the stages in case of a side-entry possibility. A, B, E and F are attachments in connection with the tension experiments, C end of heat exchanger, D thermoelement, G specimen fastening between a mobile and a stable piston.
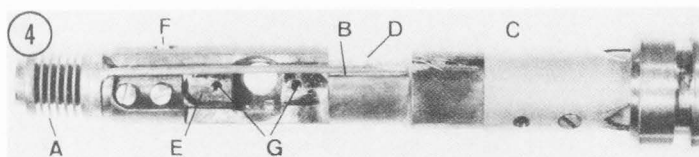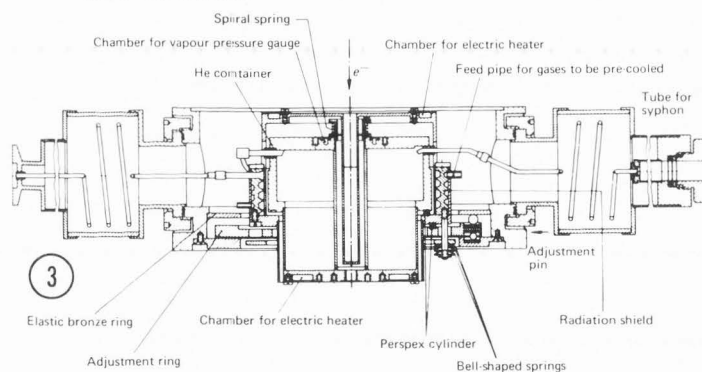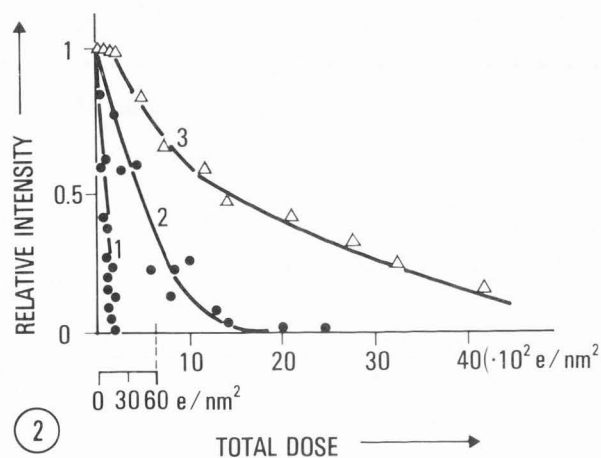
Temperatures of the order of 20 K to 30 K were obtained.

Table 1

Data of electron exposures for damaging organic materials obtained by electron diffraction at room temperature

Material	D_V (e/nm^2)	V (kV)	Reference
Chlorinated phtalocyanine	$15 - 20 \cdot 10^5$	100	Uyeda et al. (1972)
Coronene	$3 \cdot 10^3$	100	Claffey and Parsons (1972)
Cytosine	$2.5 \cdot 10^3$	20	Crewe et al. (1970)
Poly-4-methylpentene	$2 \cdot 10^2$	100	Grubb and Groves (1971)

D_V = Saturation dose, which causes the disappearance of the reflections, V = beam voltage.

be taken, only electron diffraction could be performed. Furthermore the specimen temperature in holders such as sketched in Fig. 4 was not well defined, and many authors who were aware of these difficulties just claimed that the temperature should be in a certain region e.g. between 10 and 20 K.

Since no drastic improvement in respect to radiation damage was found cold stages cooled to nearly liquid helium temperatures were mainly applied for investigating frozen specimens.

Cryostat with Superconducting Lenses

A mechanically and electromagnetically stable device which permits high resolution imaging and which guarantees a specimen temperature of $\simeq$ 4 K is a superconducting lens system. The temperature may be increased when the electron beam is switched on. Unlike cold stages the adjustment of a temperature above 4 K is here somewhat difficult (Dietrich 1976).

In Fig. 5 the construction of a cryostat with a superconducting lens system is sketched. This device can be installed in a commercial microscope with beam voltages up to 500 kV. In order to obtain the required mechanical stability, i.e. to narrow down mechanical drift and vibration, a cryostat with three chambers for cryogenic liquids was chosen. Hence it is possible to attach a sturdy connection between the chambers without producing too high of an evaporation rate. The number of feed throughs into the inner helium chamber is reduced to a minimum. The side entry specimen and aperture holders can be disconnected from the warm vacuum vessel and in this way the heat flow into the inner helium chamber is limited.

The lens system, which is supported by the wall of the inner helium chamber, consists of an objective lens of the shielding type described later and an intermediate lens with superconducting windings and an iron circuit. Superconducting coils used for stigmators and deflectors are provided. A superconducting stigmator is installed in the objective lens gap, a construction advisable only for a shielding type lens. The lens coil and most of the corrector coils are equipped with persistent current switches (Fig. 6) which permit switching off the power supply as soon as the desired excitation is obtained.

The most important part of the system is the objective lens, whose image aberration constants determine the resolution limit. The electron optically effective parts of the shown shielding lens (Fig. 7) are exclusively superconductors. The field of a superconducting coil which can be excited up to a flux density of 8 T is shaped by superconducting shielding cylinders so that a favourable field distribution results. A superconducting shielding casing prevents stray fields from penetrating into the gap. The superconducting materials applied in the lens system are NbTi multicore wire for the coils and Nb-Sn sintermaterial with the effective superconducting phase Nb_3Sn for the shielding parts. The side entry specimen holder is in touch with the shielding cylinders in order to avoid vibrations of the specimen against the lens field.

Some data of the lens systems now in operation are given in Table 2.

Results on Cryoprotection

Electron Diffraction

It was pointed out earlier that the most convenient method for the determination of the radiation damage on crystalline specimens is electron diffraction. The temperature dependence of the critical dose of two organic materials, coronene and paraffin, is plotted in Fig. 8a and b. There is not much cryoprotection between room temperature and 100 K. The cryoprotection increases more rapidly below 40 K. The diagrams provide a hint that a drastic cryoprotection should not be observed with the standard cold stages where in general a specimen temperature below 10 K is not achievable.

In Table 3 some electron diffraction results determined with cold stages are compared to those established with superconducting lens systems. The temperature values given in the table are claimed by the authors. The values of the critical doses D_e are mostly related to the fading of the first order reflections. The cryoprotection factor or gain $G = D_e(4\ K)/D_e(300\ K)$ amounts to $G \leq 5$ in the case of cold stages while $G \simeq 6$ up to 300 was obtained with superconducting lens systems. This discrepancy in the results is not only attributable to the somewhat different temperatures but also to preparation methods used by some authors which apparently were not suitable for work at low temperatures. Furthermore pronounced dose rate effects were discovered with some materials, even if they were mounted on suitable support films (e.g. $[Cu_2BSH]_n$), i.e. the density of the electron current also determined the damage rate. These problems are discussed below.

The D_e values indicate the maximum dose, which should be taken for direct images if the lattice distances related to the reflections whose fading was measured are to be resolved. In this way one has a criterion in order to decide if one has a chance to achieve micrographs with sufficient contrast at the magnification necessary for the desired resolution.

Direct Images

Successful high resolution imaging with cold stages was only performed in the aforementioned case of the purple membrane, where the specimen was embedded in vitreous ice. Since the specimen temperature was 150 K no actual cryoprotection could take place. The specimens were exposed to a dose of $\simeq$ 100 e/nm^2.

Some interesting facts about direct images taken with superconducting lens systems can be learned from Table 4. The electron optical data of the electron microscopes are listed in Table 2.

The results presented in Table 4 besides those of hexaphenylene mercury, murein and $[Cu_2B-SH]_n$ are preliminary. Nevertheless it is possible to draw the conclusion that a resolution of 0.3 nm can be achieved on unstained specimens even with a dose of 3000 e/nm^2.

We discuss here in more detail the images of the crystalline copper complex N,N'-bis-salicyloyl-hydrazine $[Cu_2BSH]_n$ spread on holey carbon foil (Fig. 9) and of murein prepared on graphite oxide which is supported by a holey carbon foil (Fig. 10). The integral dose applied for high resolution imaging of $[Cu_2BSH]_n$ (Fig. 11a) corresponds
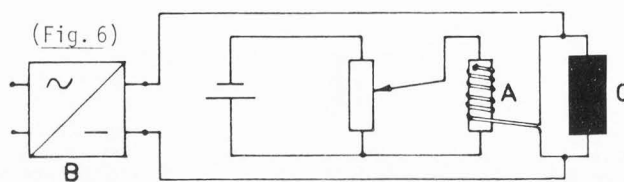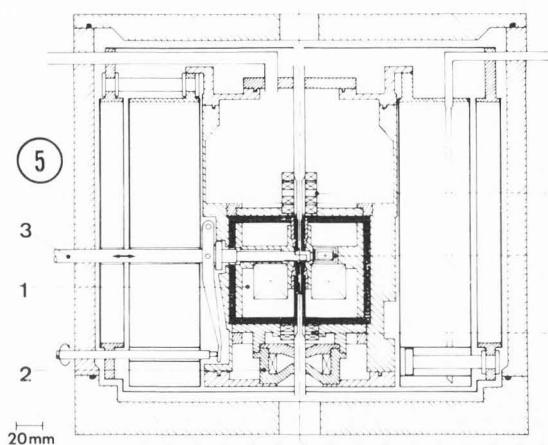
Fig. 5. Superconducting lens system (Dietrich 1978). (1) objective lens, (2) intermediate lens, (3) side entry specimen holder, (4) correction systems.

Fig. 6. Persistent current switch. For exciting the superconducting coil C by the current generator B the heater A has to be switched on so that the left part of the coil circuit becomes normal. As soon as the desired field strength is obtained the heater is switched off and a persistent current flows in the closed superconducting coil circuit.
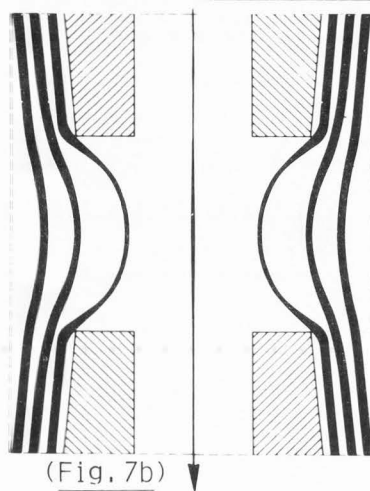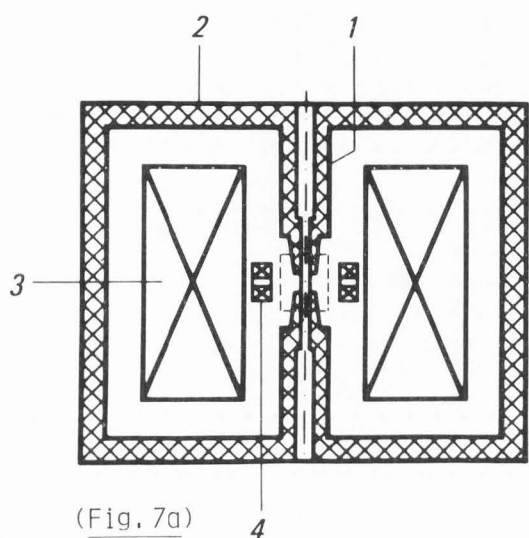
(Fig. 7a)

Fig. 7. Superconducting shielding lens. (a) construction principle (1) shielding cylinders (Nb-Sn sinter material) (2) shielding casing (Nb-Sn sinter material) (3) coil (Nb-Ti multicore wire) (4) stigmator coils (50 μm thick Nb-Ti single core wire) (b) field distribution in the gap.
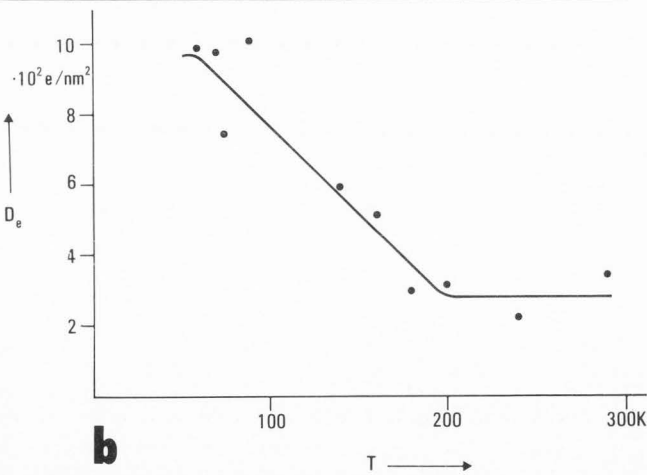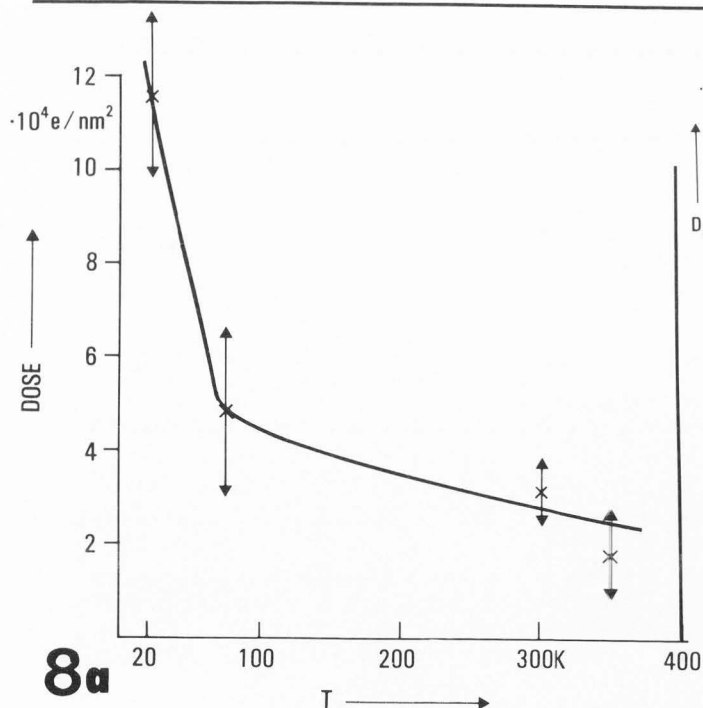
(Fig. 7b)

b

8a

Fig. 8. Variation with temperature of the critical dose D_e measured by electron diffraction technique. a. Coronene, beam voltage 500 kV (Salih and Cosslett 1975). b. Paraffin, beam voltage 80 kV, scanning transmission microscope (Freeman et al. 1980).

I. Dietrich, E. Knapek, and G. Lefranc

Table 2

Data of super conducting lens system

	Units	System I	System II
Applied beam voltage V	kV	230	125
Focal length f	mm	1.8	1.7
Chromatic aberration const.	mm	1.3	1.3
Spherical aberration const.	mm	1.45	1.2
Gap	mm	4	7.5
Coil exitation time	min	30	8
Basic astigmatism $\Delta f/f$		1.5 %	1.5 %
Diameter of specimen grid	mm	1.5	3
Drift	nm/min	0.03	0.05
Positioning reproducibility	nm	1,000	50
Point to point resolution: calculated	nm	0.14	0.15
measured	nm	0.15	0.3
He consumption: cooling down	1	5	2.5
operation	1/h	1.5	1
Specimen temperature without irradiation	K	4	4

Till today three superconducting lens systems, which permit one to take high resolution micrographs, are in operation. System I, which contains four superconducting lenses, is part of a 400 kV microscope set up in the Siemens research laboratories in Munich. Most of the investigations reported here were performed with System I.

One of the two tested Systems II (Fig. 5) is working in the Fritz Haber Institute, Berlin, where it is attached to a laboratory device of the Siemens CT 150 microscope, and the other has been installed in a Zeiss EM 10 at the European Molecular Biology Laboratory, Heidelberg recently.

Table 3

Increase of damage dose due to specimen cooling measured by electron diffraction

	Cold stages		Superconducting lenses				
Specimen	Estimated temp. K	Low temp. to room temp. improvement	D_e (300 K) e/nm^2	D_e (4 K) e/nm^2	$\frac{D_e \, (4 \, K)}{D_e \, (300 \, K)}$	Remarks	Reference
L-valine	10-20	1	30				Glaeser (1971)
				2,000	60	System I	Knapek and Dubo-chet (1980)
				1,500		System II	Müller et al. (1981)
Polyethylene	18	3	150				Grubb and Groves (1971)
				4,000	30	System I	Knapek (1982)
				4,000		System II	Müller et al. (1981)
Adenosine	10-20	1.5	60				Glaeser et al. (1971)
				20,000	350		Knapek and Dubo-chet (1980)
Paraffin	4	4	380				Siegel (1972)
				11,000	30	System I	Knapek and Dubo-chet (1980)
				5,000		System II	Müller et al. (1981)

D_e = critical dose which causes a fading of the intensity of the reflections by a factor e; System I, System II, see Table 2.
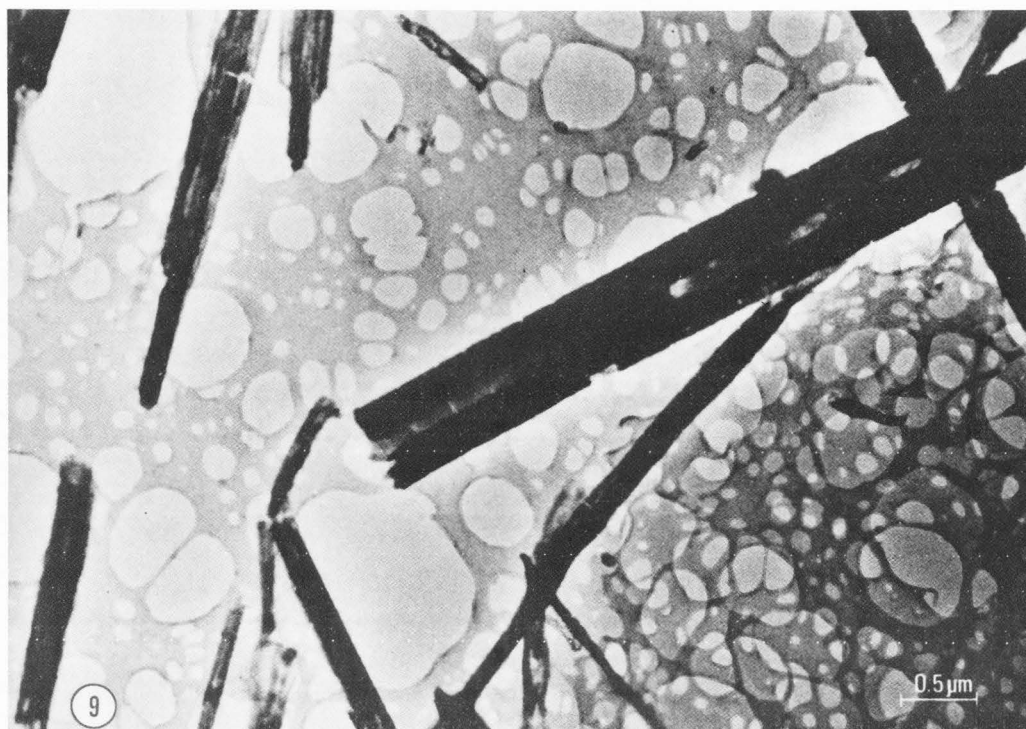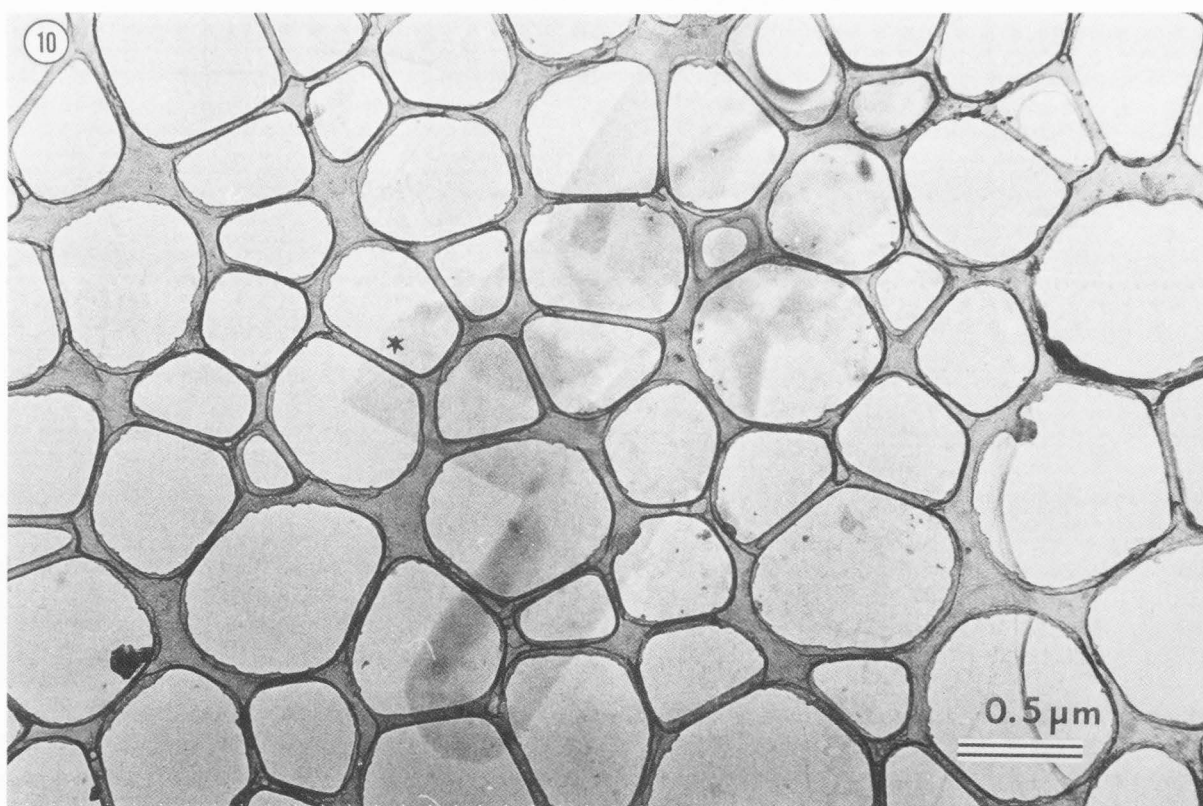
Fig. 9. $[Cu_2BSH]_n$ crystals on holey carbon foil carriers. Survey micrograph, beam voltage 220 kV (Dietrich et al. 1982).

Fig. 10. Saculi of murein on holey carbon foil carriers covered with graphite oxide. The star marks the location of a murein single layer (Dietrich et al. 1979).
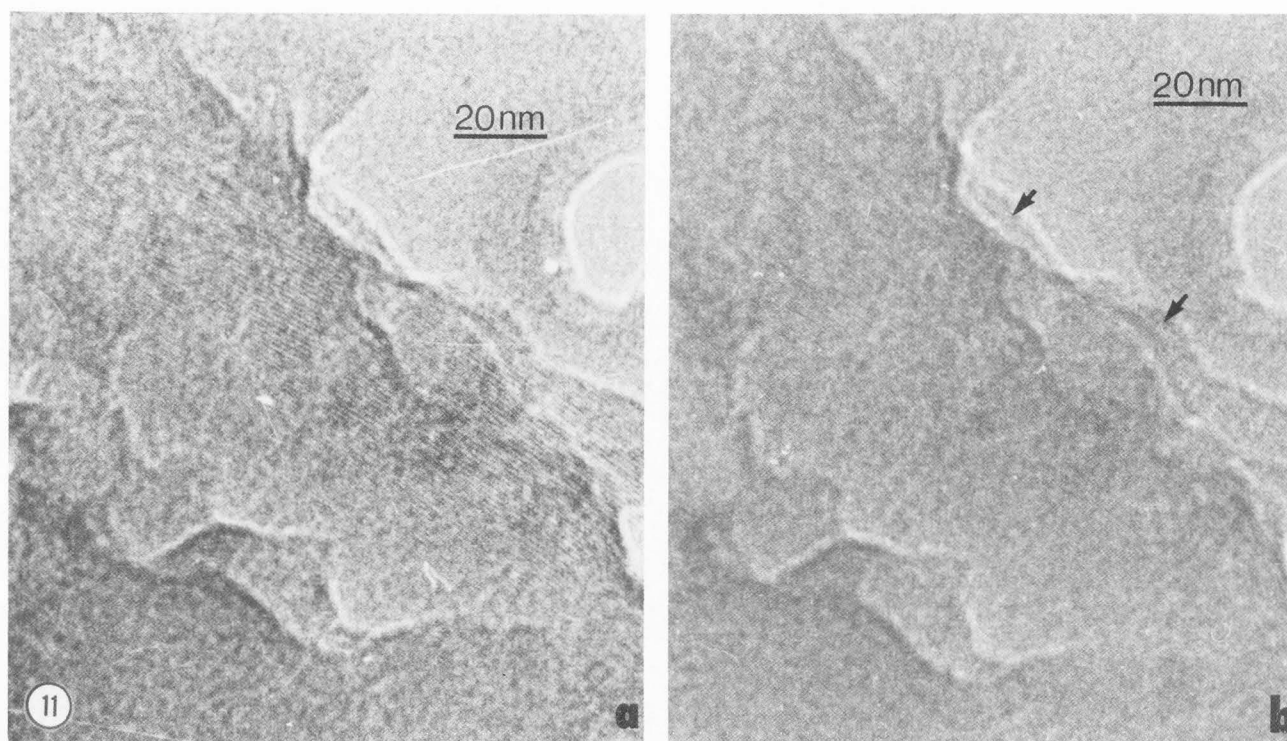

355

Fig. 11. High resolution image of $[Cu_2BSH]_n$. Electron optical magnification 80,000x, dose rate 400 e/nm^{2}s, beam voltage 220 kV, object temperature $\simeq$ 4K. a. Integral dose 35,000 e/nm^2. The 1.1 nm lattice lines are clearly visible. b. Integral dose 55,000 e/nm^2. The start of damage is indicated by arrows. c. Integral dose 75,000 e/nm^2. The lattice lines have disappeared.

Table 4

Results of direct imaging with superconducting lenses

Material	Support film	Previous electr. diffr. experim. D_e (4 K) e/nm^2	1/R nm	Micro-scope EM x 10^3	Dose D_i e/nm^2	D_v e/nm^2	Dose rate e/nm^2·s	Photogr. emulsion	Resolved distance nm	Specimen prepared by	Reference
Hexaphenylene mercury	amorphous aluminium oxide			M 400				A	0.36	Formanek	Formanek and Knapek (1979)
Murein	graphite oxide			M 86	$3 \cdot 10^5$	$1.5 \cdot 10^6$	$3 \cdot 10^2$ 10^4	A	0.45(0.22)	Formanek	Dietrich et al. (1979)
Catalase	carbon			M 40	$2.5 \cdot 10^5$	$7.5 \cdot 10^5$		A	6.8(2.9)	Dubochet	Knapek and Dubochet (1980)
$[Cu_2BSH]_n$	carbon	12,000	0.4	M 80	$3 \cdot 10^4$	$7.5 \cdot 10^4$	10^2	A	1.1, 0.9	Formanek	Dietrich et al. (1982)
Cellulose	carbon	1,000	0.54	M 50	1,000		80	A	0.54	Chanzy	Lefranc et al. (1982)
Paraffin	carbon	11,000 7,000	0.415 0.375	M 60	3,000	4,000	100	K	0.41, 0.37	Dorset	
Coronene	carbon			B 40	9,500			A	0.7	Fryer	Fryer et al. (1982)
Purple membrane	carbon	1,200		B 45	2,000			A	1.8	Studer	Studer et al. (1982)
Crotoxin	carbon	1,000	0.3	B 40	1,200		15	K	0.9	Chiu	Chiu et al. (1982)

D_e is the dose which causes a decrease of the intensity of the reflection R by a factor e, where 1/R is the interlattice-plane distance. EM = electron optical magnification.
M and B mean the micrographs were taken in the 400 kV test microscope in Munich (System I) and the 125 kV microscope with superconducting lens system in Berlin respectively. D_i is the dose used for imaging and D_v the saturation dose which causes a complete disappearance of the reflections. The emulsion A is Agfa Scientia, K is Kodak electron image film 4463.
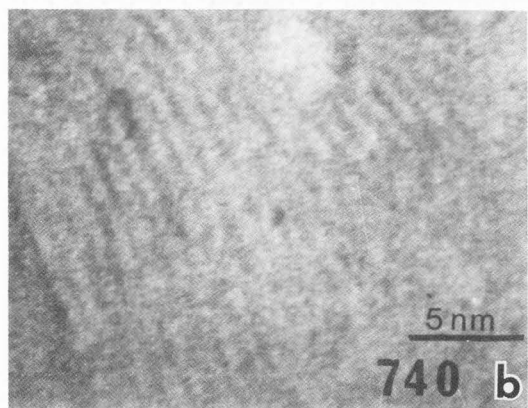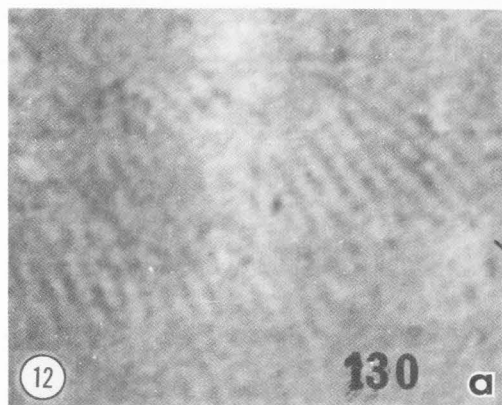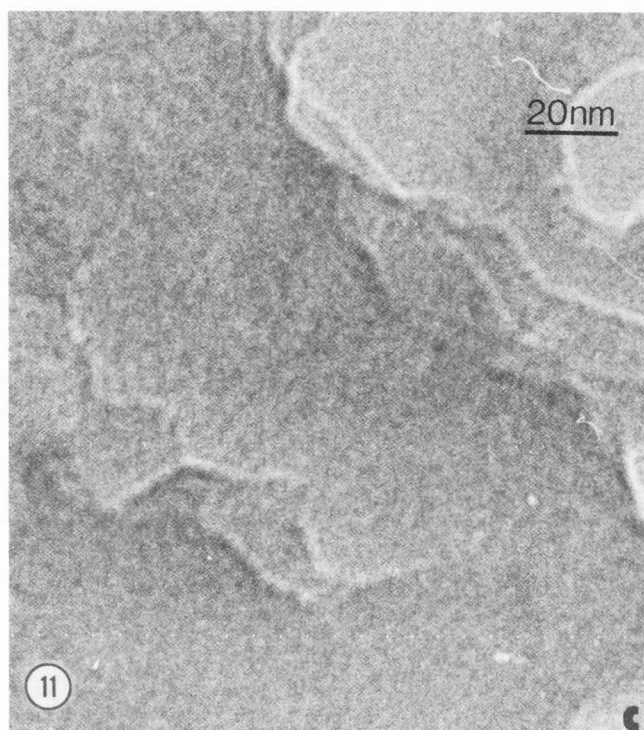
Fig. 12. Small $[Cu_2BSH]_n$ crystals embedded in a quasi-amorphous matrix of the same material. Data see Fig. 11. a. Integral dose 13,000 e/nm². b. Integral dose 74,000 e/nm².

to the D_e value of this compound (Table 4). The imaged crystal lies on top of the carbon foil, and predictions about the thermal contact are not possible. For micrograph Fig. 11b the specimen was exposed to a somewhat larger dose. One can clearly recognize that the fading of the lattice lines starts at the edges of the crystal. The consequence of an even higher dose rate is the complete destruction of the crystal (Fig.11c) while if small crystals of $[Cu_2BSH]_n$ are embedded in an amorphous material this scarcely changes the imaged lattice, because the radiation protection has been improved (Fig. 12a, b).

The same behaviour can be discovered on the micrographs of murein, the rigid layer of the cell wall of the bacterium spyrillum serpens. The stability against radiation damage is here very high partly due to specific staining with platinum. But in addition, all the crystalline parts visible on Fig. 13a are surrounded by amorphous material of the same chemical composition. The decline of the crystals in these specimens also starts from the edges whereas a very high dose and dose rate has to be applied (Fig. 13b).

The goal of high resolution electron microscopical investigations on organic materials is in general to determine their steric structure or to confirm an already existing hypothetical structure. We have succeeded twice in achieving this purpose. With the help of direct images single crystal diffraction patterns and some chemical knowledge, a model of the $[Cu_2BSH]_n$ structure could be constructed (Fig. 14a, b). Several murein models have been published. One of them, proposed by Formanek et al. (1974), was confirmed by the images in Fig. 13. The model (Fig. 15) is characterized by an especially dense packing and as a consequence the highest intensity in the points of the reciprocal lattice should be coordinated to distances of 0.45 nm. Just these distances appear in the image Fig. 13.

With the possibility of a reduction of radiation damage by cooling one should be more successful in the atomic structure analysis of organic material in the future.

Hints on the Preparation of Organic Materials for Effective Cryoprotection

In the last section it was already mentioned that the preparation methods in general for conventional electron microscopy cannot be applied for 4 K investigations. Fig. 16 indicates what may happen if the specimen carriers consist of formvar or a similar material. The thermal and electrical conductivities of these support films are extremely low at 4 K and hence heating and charging by the electron beam can occur which does not take place at room temperature. This is the reason why the critical dose of crystals mounted on formvar largely depends on the dose rate, i.e. the electron current density, and furthermore the thickness of the paraffin crystals and the distance of the crystals under observation from a crossbar of the copper net. Fig. 16 demonstrates that under unfavorable conditions nothing may be gained by cooling the specimen. With carbon carriers, however, whose thermal and electrical conductivities are reasonable, an average gain of $\simeq 30$ could be re-

(Fig. 14a)

Fig. 14. Structure model of $[Cu_2BSH]_n$. Z-shaped boards are used for symbols of BSH with attached Cu. a. Z-shaped board with the BSH formula. b. Model of the polymer.
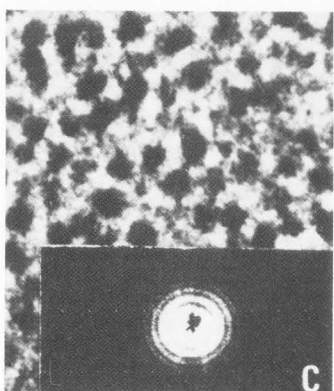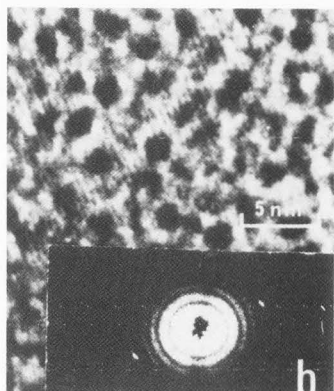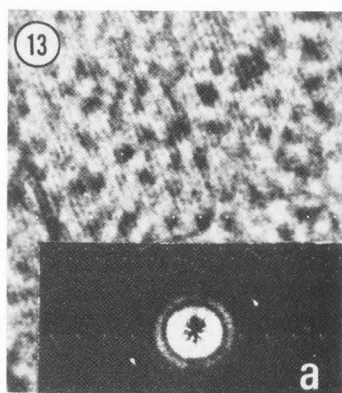
Fig. 13. Images of 0.45 nm lattice lines of murein specifically stained with Pt and light optical diffracto-grams. Electron optical magnification 80,000, beam voltage 220 kV, object temperature 4 K. a. Integral dose 60,000 e/nm², dose rate $3 \cdot 10^2$ e/nm²s. b. Integral dose 360,000 e/nm², dose rate $3 \cdot 10^2$ e/nm²s. c. Integral dose 1,500,000 e/nm², dose rate for two thirds of the dose $5 \cdot 10^3$ e/nm²s.
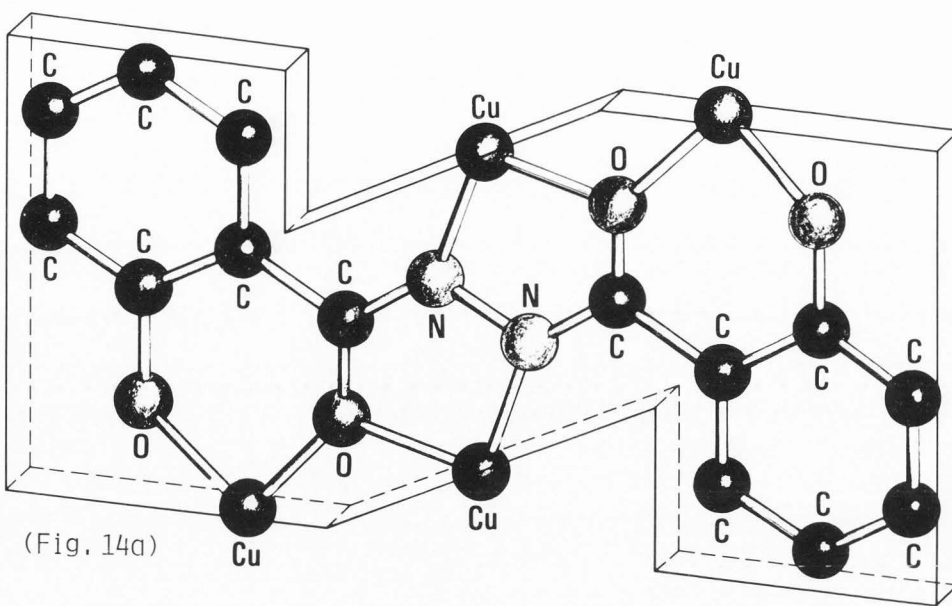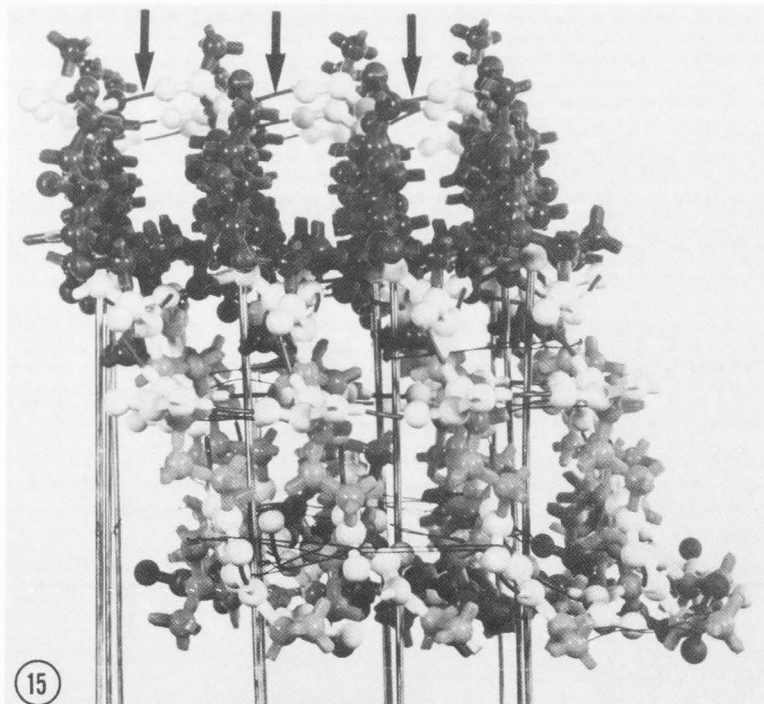

Fig. 15. Formanek's model of murein. A network of polysaccaride strains with a distance of 0.45 nm (between the arrows in the upper part) is connected with peptide chains (lower part).
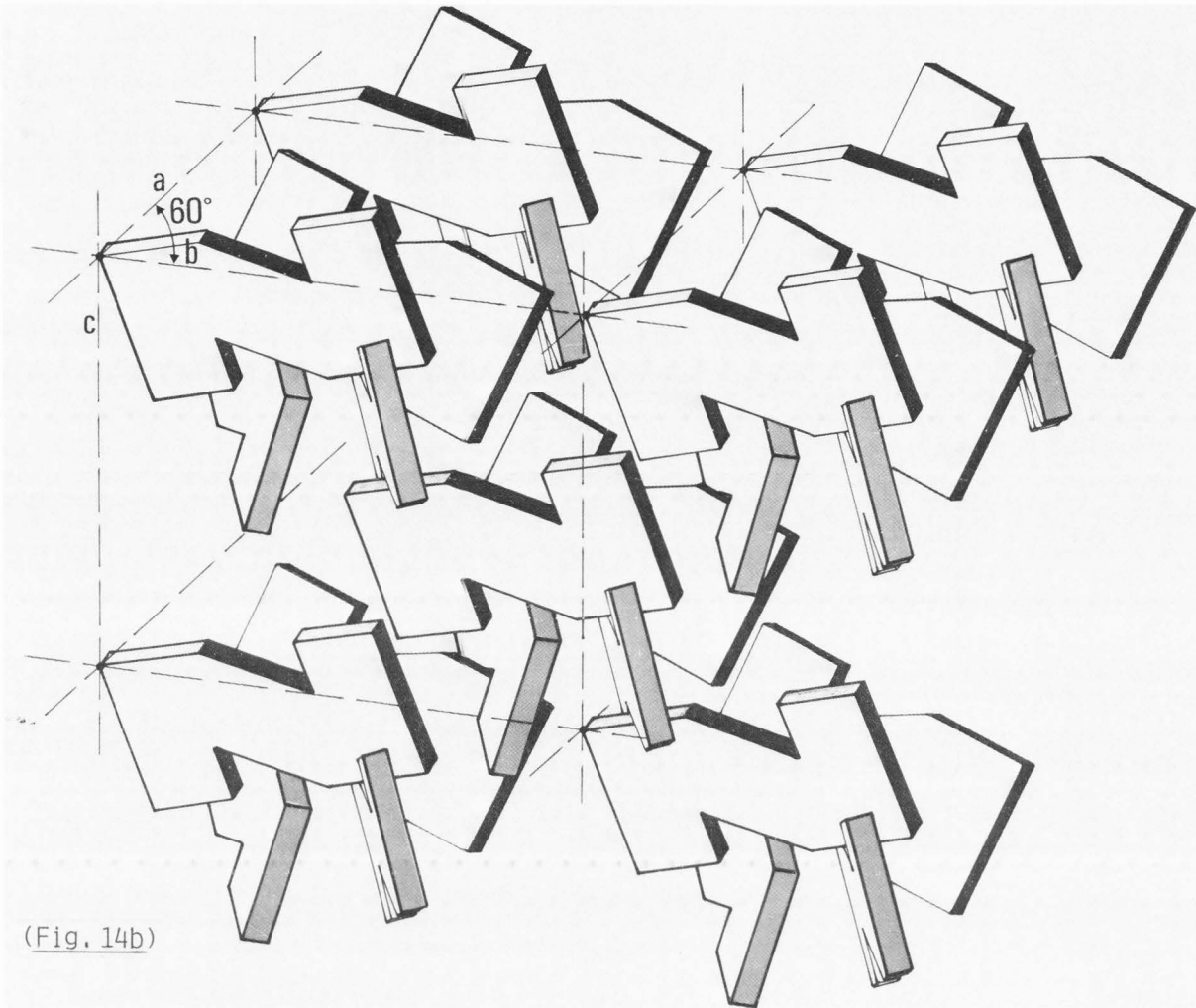
(Fig. 14b)

Fig. 16. Dose rate dependence of critical dose D_e of paraffin crystals on formvar film investigated by electron diffraction. Beam voltage = 220 kV, object temperature = 4 K. (1) Paraffin crystals on carbon foil at 4 K for comparison. (2) Thin paraffin crystals near a rod of the copper carrier net. (3) Thin paraffin crystals in some distance from the copper rod. (4) Thick paraffin crystals. (5) Paraffin crystals on carbon foil at 300 K for comparison.
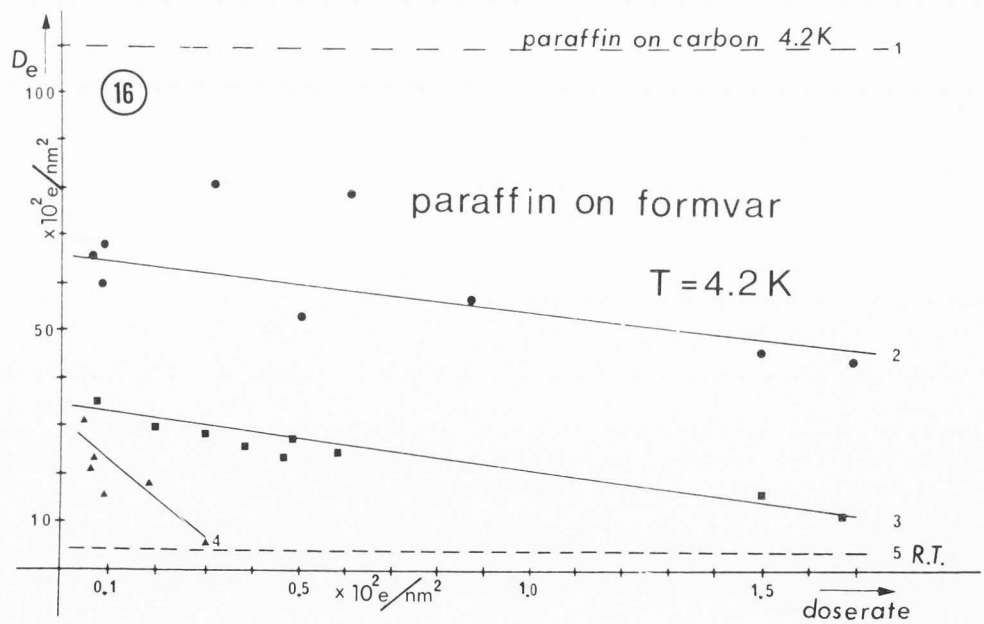
produced independently of the dose rate and the location of the crystals. This result is confirmed by investigations of the crotoxin complex where a gain of ≃ 10 was established due to cooling to 4 K as long as carbon-coated formvar carriers were used. A change to carbon film supports increased the gain to 50 (Chiu et al. 1982).

Preparation of the specimen on electrically insulating films may even prevent low temperature electron microscopy entirely since the films may burst due to electrostatic forces or the details which should be observed change their position permanently as a consequence of charging by the beam.

It seems to have been proven in the meantime that embedding of the specimen may increase the cryoprotection. Embedding is a standard preparation procedure of biologists, who often use glucose for stabilizing unstained biological material. Another method which is only mastered by a few laboratories is shock freezing of samples which were dipped into water. The cold specimens have to be transferred into the microscope and investigated in the cold state (~ 100 K). There are indications that embedding in vitreous ice works well for 4 K experiments, while glucose, which is radiation-sensitive itself even at low temperatures, apparently hinders the cryoprotection. Preliminary experiments with L-valine embedded in carbon permit the conclusion that in comparison with objects where crystals are spread on top of a carbon foil, the cryoprotection is enhanced.

Hence we can summarize that a high cryoprotection factor can be obtained if the specimen is mounted on supports whose thermal and electrical conductivities are not too low. A further improvement can be expected by embedding. In case this cannot be done, e.g. if self-carrying well insulating membranes are to be investigated, the dose rate has to be reduced to a minimum.

Possible Reasons for the Temperature Influence on Radiation Damage

In the last sections we have described some experiments which prove the existence of cryoprotection on the investigated materials in electron microscopy. But a good theory which explains this fact is not at our disposal. Low temperature investigations provide some hints, so that we can begin to anticipate the connections.

According to radiochemical investigations of special organic compounds (e.g. Box 1975) with electron spin resonance (ESR), in particular at 4 K, the primary effects in radiation damage as described in the introduction take place in the same way as at 300 K, but the secondary processes which are connected with the migration of ions are prevented completely, and for this reason no structure changes occur below 10 K. At 10 K, however, the diffusion of ionized hydrogen starts and hence the originally stable structure may weaken.

The radiochemical findings were confirmed by electron microscopical experiments on paraffin as far as the primary effects are concerned. In fact the exposure of the object at 4 K apparently causes the latent damage, and further warming up brings about the same damage as irradiation at

higher temperature (Siegel 1971).

The relatively low cryoprotection at temperatures of the order of 10 K or somewhat above can also be made plausible by the ESR measurements, since the electron impact should produce free hydrogen ions. This result was confirmed by Parkinson et al. (1980). Partial pressure measurements of hydrogen were performed in an electron microscope with an attached mass spectrometer. The H-pressure increased when the temperature of the irradiated organic specimen was raised above 10 K.

A further statement, however, of the radiochemical analysis is that no visible second-order effects should occur at 4 K. This does not apply for electron microscopy. Pointers to what may happen can be taken from the investigations on phonon processes at low temperatures. At the phase boundaries between specimen and vacuum and specimen and carrier foil thermal contact resistances are orders of magnitude higher than at 300 K and the phonons produced by the electron impact are reflected. Standing waves with a high energy density may be the consequence, which should produce lattice defects. Such defects are the starting points for further damage, as can be seen in the micrographs of Fig. 1. The fact that the decay of organic lattices due to electron impacts starts at the edge (Fig. 11a, b) and that embedding increases the cryoprotection (Fig. 12a, b) gives a certain realistic background to the hypothesis of the phonon influence.

Acknowledgement

References

Box HC. (1975). Cryoprotection of irradiated specimens, in: Electron Microscopy and Microbeam Analysis, B.M. Siegel and R. Beam (eds.), John Wiley and Sons, New York, 259-285.

Chiu W, Jeng T, Brakmo L, Müller K-H, Knapek E, Stemmer A, and Zeitler E. (1982). Electron microscopy of unstained, hydrated protein crystals at 4 K, Proc. 10th Int. Congr. El. Microsc., Hamburg, Deutsche Gesellschaft für Elektronenmikroskopie, Frankfurt, vol. II, 453-454.

Claffey WJ, Parsons DF. (1972). Electron diffraction study of radiation damage in coronene, Phil. Mag. 25, 635.

Crewe AV, Isaacson M, and Johnson D. (1970). Electron beam damage in biological molecules. Proc. 30th Ann. EMSA Con. (Los Angeles), Claitor's Publishing Div., Baton Rouge, LA, 384-385.

Dietrich I. (1976). Superconducting Electron-Optic Devices, K. Mendelssohn and K.D. Timmerhaus (eds.), Plenum Press, New York.

Dietrich I. (1978). Superconducting lenses, Proc. 9th Int. Congr. El. Microsc., vol. III, Microscopical Society of Canada, Toronto, 173-184.

Dietrich I, Formanek H, Fox F, Knapek E, and Weyl

R. (1979). Reduction of radiation damage in an electron microscope with superconducting lens system, Nature 277, 380-381.

Dietrich I, Formanek H, von Gentzkow W, and Knapek E. (1982). Structure determination of an organic copper complex with a superconducting electron microscope, Ultramicroscopy, 9, 75-84.

Formanek H, Formanek S, and Wawra H. (1974). A three-dimensional model of the murein layer of bacteria, Eur. J. Biochem. 46, 279-294.

Formanek H, Knapek E. (1979). Bright-field imaging of single heavy atoms in an electron microscope with superconducting lens system, Ultramicroscopy 4, 77-84.

Fryer JR, Müller K-H, Stemmer A, and Zeitler E. (1982). High resolution studies of organic crystals at 4 K, Proc. 10th Int. Congr. El. Microsc., Hamburg, Deutsche Gesellschaft für Elektronenmikroskopie, Frankfurt, vol. II, 451-452.

Freeman R, Leonard KR, and Dubochet J. (1980). The temperature dependence of beam damage to biological samples in the scanning transmission electron microscope, Proc. 7th Europ. Congr. El. Microsc., The Hague, vol. 2, 7th Europ. Congr. El. Microsc. Foundation, Leiden, The Netherlands, 640-641.

Glaeser RM. (1971). Limitations of significant information in biological electron microscopy as a result of radiation damage, J. Ultrastruct. Res. 36, 466-482.

Glaeser RM, Cosslett VE, and Valdré U. (1971). Low temperature electron microscopy: radiation damage in crystalline biological material, J. Microscopie (Paris) 12, 133.

Grubb DT, Groves GW. (1971). Rate of damage of polymer crystals in the electron microscope: dependence on temperature and beam voltage, Phil. Mag. 24, 815-827.

Haywardt SB, Stroud RM. (1981). Projected structure of purple membrane determined to 3.7 Å resolution by low temperature electron microscopy, J. Mol. Biol. 151, 491-517.

Isaacson MS. (1977). Specimen damage in the electron microscope, in: Principles and Techniques of Electron Microscopy. Biological Application, M.A. Hayat (ed.), Van Nostrand Reinhold Co., New York, 3-78.

Knapek E. (1982). Properties of organic specimens and their supports at 4 K under irradiation in an electron microscope. Ultramicroscopy, 10, 71-86.

Knapek E, Dubochet J. (1980). Beam damage to organic material is considerably reduced in cryo-electron microscopy, J. Mol. Biol. 141, 147-161.

Lefranc G, Knapek E, and Dietrich I. (1982). Construction principles for stable superconducting lens systems as required for obtaining high resolution images, Proc. 10th Int. Congr. El. Microsc., Hamburg, Deutsche Gesellschaft für Elektronenmikroskopie, Frankfurt, vol. I, 391-392.

Müller K-H, Zemlin F, and Zeitler E. (1981). Cryoprotection of electron-irradiated organic crystals,

Proc. 39th Ann. EMSA Con., Claitor's Publishing Div., Baton Rouge, LA, 26-27.

Murata Y. (1978). Studies of radiation damage mechanism--by optical diffraction analysis and high resolution imaging, Proc. 9th Int. Congr. El. Micr., vol III, Microscopical Society of Canada, Toronto, 49-60.

Parkinson GM, Jones W, and Thomas JM. (1980). Electron microscopy at liquid helium temperature, in: Electron Microscopy at Molecular Dimensions, W. Baumeister and W. Vogell (eds.), Springer, Berlin, 208-225.

Salih SM, Cosslett VE. (1975). Radiation damage in electron microscopy of organic materials: effect of low temperatures, J. Microsc. 105, 269-276.

Siegel G. (1972). Der Einfluß tiefer Temperaturen auf die Strahlenschädigung von organischen Kristallen durch 100 keV-Elektronen, (The influence of low temperatures on the radiation damage of organic crystals by 100 kV electrons). Z. Naturforsch. A 27, 325-332.

Studer D, Gross H, Stemmer A, and Müller K-H. (1982). Cryo-electron microscopy of purple membrane, Proc. 10th Int. Congr. El. Microsc., Hamburg, Deutsche Gesellschaft für Elektronenmikroskopie, Frankfurt, Vol. II, 455-456.

Thomas P, Louchet F, Kubin L, and Jouffrey B. (1974). Porte-objet de traction refroidi par l'hélium liquide adaptable sur un microscope éléctronique a très haute tension, (object carrier for tension experiments cooled with liquid helium adaptable to an electron microscope for very high voltages). Proc. 8th Int. Congr. El. Microsc., vol. 1, Australian Academy of Sci., Canberra, 176-177.

Unwin PNT, Henderson R. (1975). Molecular structure determination by electron microscopy of unstained crystalline specimens, J. Molec. Biol. 94, 425-440.

Uyeda NT, Kobayashi T, Ohara M, Watanabe M, Taoka T, and Harada Y. (1972). Reduced radiation damage of halogenated copper-phtalocyanine, Proc. 5th Europ. Congr. El. Microsc., Manchester 1972, Inst. Physics, London, 566-567.